Confrontation between Structural and Thermal Properties of $Ni_XTi_{X-Y}Hf_Y$ .at% Ternary Alloys Obtained by three Distinct Fusion Processes

Roniere Leite Soares
Federal University of Campina Grande
UFCG – CCT – UAEP - AEG
Campina Grande – Paraíba - Brazil

Walman Benício de Castro
Federal University of Campina Grande
UFCG – CCT – UAEM - LaMMEA
Campina Grande – Paraíba - Brazil

Abstract:- **The present research focused on the experimental results obtained for the $Ni_XTi_{X-Y}Hf_Y$ .at% (where X = 50; Y = Hf = 8, 11, 14, 17 and 20 .at%) substitutive alloys with shape memory effect (SME). The samples were fused by 3 different processes and subjected to X-Ray Diffraction (XRD) and differential scanning calorimetry (DSC) to demonstrate the differences between structural and thermal properties for equal compositions. In addition, chemically etched samples were used for surface observation in two types of microscopy: optical microscopy (OM) and scanning electron microscopy (SEM). The results derived from the three distinct processes were compared and discussed, confirming several significant differences in the properties studied here.**

Keywords:- *DSC; Microscopy; Ni-Ti-Hf; Ternary Alloys; XRD.*

I.   INTRODUCTION

In Shape Memory Alloys (SMA), is common to find studies of Transformation Temperature (TTs) and (micro)structural characteristics for a given composition that include: grains, grain boundaries, polycrystallinity, size of crystallite (crystalline domain), stoichiometric formation, phases crystallographic features, space groups, relative degree of crystallinity, crystalline planes indexation, amorphous content, etc. [1]. However, for a given nominal (theoretical) composition, subjected to differentiated processes, these material characteristics may vary. This can determine a material with greater or lesser suitability, depending on the application for which the material was designed / developed.

According to Figure 1, three processes were used in the casting of $Ni_xTi_{x-y}Hf_y$ .at% SMA alloys: ① Plasma arc melting with a Discovery All Metal furnace from EDG (PSPP method) [2]; ② Melt spinning [frequencies from 30 Hz to 40 Hz] [3]; and ③ electric arc melting [4].
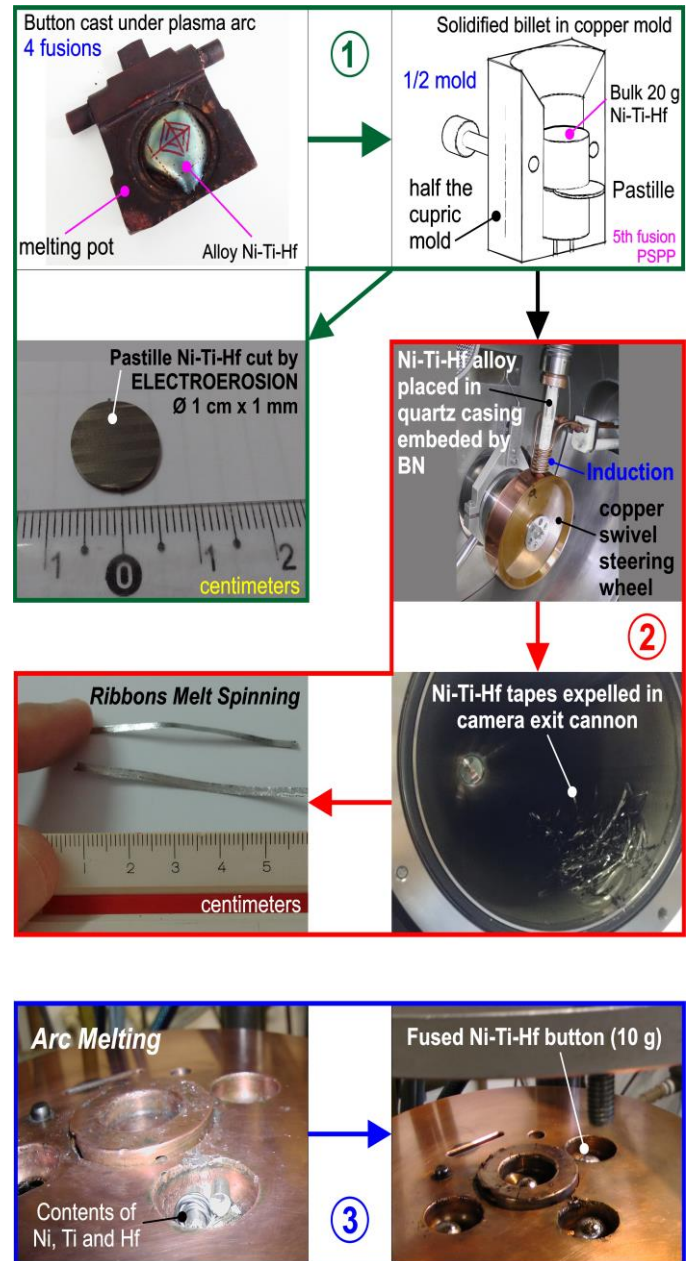

Fig 1:- Sequences for each of the three methods to obtain the NixTix-yHfy .at% alloy (x = 50; and y = Hafnium = 8, 11, 14, 17 and 20 .at%)

II. DEVELOPMENT

Based on experimental results, it was possible to compare between microstructural and thermal characteristics observed in alloys with the same nominal composition but obtained by different processes. According to the XRD analysis in Figure 2, it is possible to see that certain phases, present for a giver composition, are identical (are aligned to the same 2θ at the diffractograms), regardless of the processing involved. However, the intensity of these phases in each process depend on the peculiar variables applied during production and also on the experimental conditions applied. Even so, there are new phases for equal nominal compositions $Ni_XTi_{X-Y}Hf_Y$ .at%.
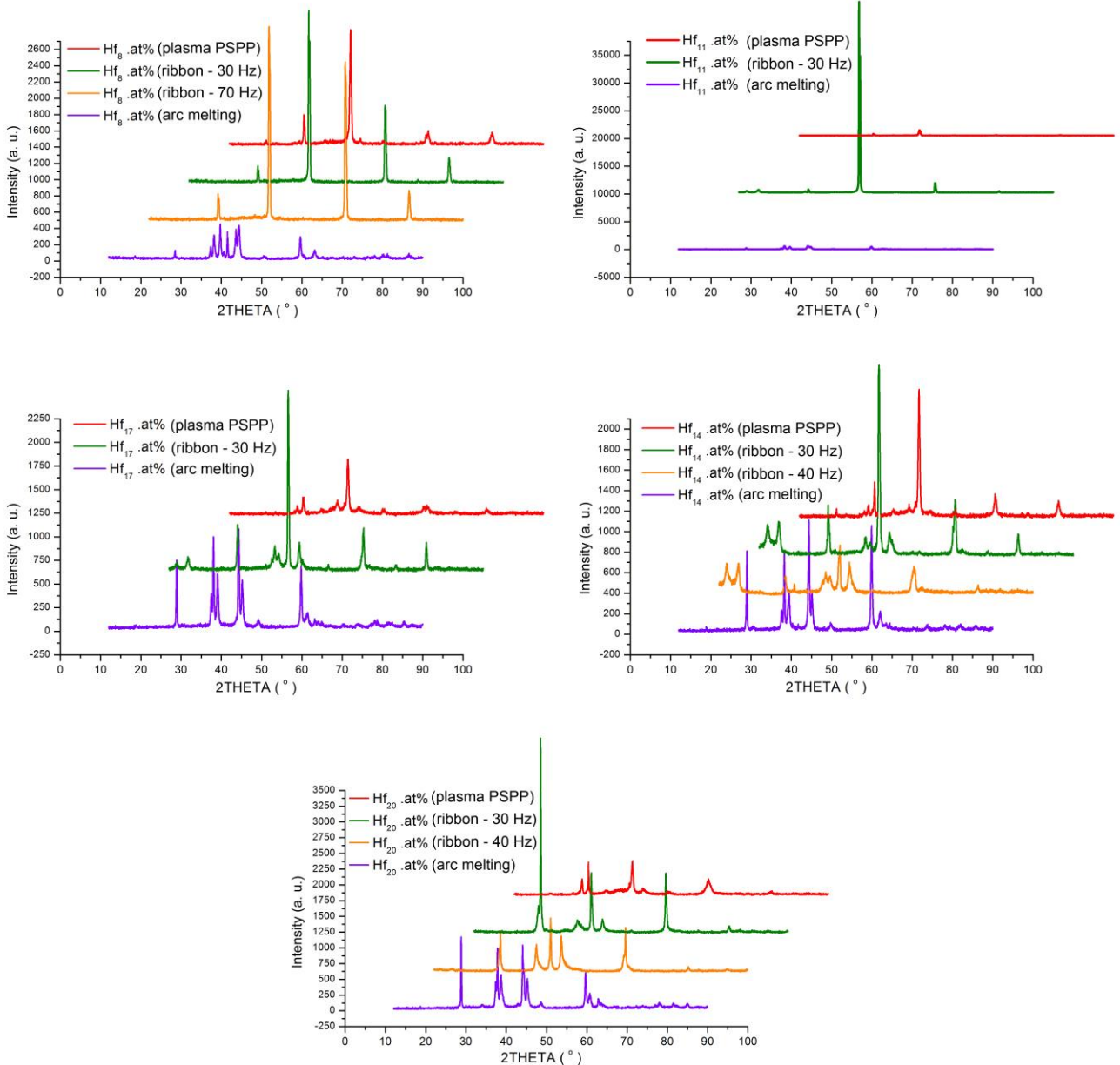

Fig 2:- Comparison between coincident phases and new phases obtained from different nominal compositions (Y = 8, 11, 14, 17, 20 .at%)

Regarding the identified phases, there is a greater incidence, both mass and volumetric, of martensitic B19' phases (monoclinic) in all three processing routes adopted [5]. However, these phases are more evident after the arc melt process, with higher percentual relative crystallinity (X_c).

Regarding the (micro)structural characterization, carried out at room temperature, it is possible to state that, even though these alloys are polycrystalline materials (which present varied structures, with distinct spatial groups), there is a decreasing exponential (negative) relationship between the interplanar distance (or d-spacing) and Bragg angle 2θ (°) [6]. However, in relation to the fraction $1/d^2$, which identifies the crystal, the quadratic

relationship to the angle 2θ is increasing (positive). In this sense, it was possible to establish mathematical models capable of calculating the d value for all 3901 points detected in the XRD experiments. Table 1 presents the general equations for the various nominal compositions, considering the processing individually. The proximity between the values of the functions and the R^2 values are always greater than 0.99 and express how valid the adjustments of the said exponential function ($f(d) = y_0 + Ae^{R_0 x}$) and quadratic function ($f\left(1/d^2\right) = \beta_0 X^2 + \beta_1 X + \beta_2 \pm \varepsilon$) were. The constant e represents Euler's number, expressed by $e = \lim_{n \to \infty}\left(1 + \frac{1}{n}\right)^n$ and is approximately 2,1782.

With these functions it is possible to calculate the d spacing values for all 3901 experimental points. The results provided by the Shimadzu XRD-600 equipment, restricted to some values of interplanar distances (d), would be insufficient for the plotting of XRD diffractograms representing d x Intensity (a.u).

Regarding the phase transformation temperatures (TTs), we take as an example the nominal compositions $Ni_{50}Ti_{36}Hf_{14}$ .at% and $Ni_{50}Ti_{30}Hf_{20}$ .at%, accordingly to Table 2. There was a growth in all TTs, according to the order of processing used, namely: melt spinning (lower TTs), plasma arc melting (median TTs), electric arc melting (higher TTs). In the case of tapes solidified by melt spinning, there was a decrease in TTs when the frequency of the rotating flywheel increased from 30 Hz to 40 Hz. Both speeds refer, respectively, to 18.84 m/s and 25.83 m/s.

Processing	Exponential		Quadratic	
	d	**Value**	**1/d^2**	**Value**
Plasma arc (*PSPP method*)	y_0	1.1117	β_0	-0.0424
	A	8.93061	β_1	0.00299
	R_0	0.05158	β_2	7.97E-05
Rapid solidification (*melt spun*)	**d**	**Value**	**1/d^2**	**Value**
	y_0	1.22438	β_0	-0.03312
	A	11.76312	β_1	0.00248
	R_0	-0.06197	β_2	8.33E-05
Electric arc (*arc melting*)	**d**	**Value**	**1/d^2**	**Value**
	y_0	1.07036	β_0	-0.06822
	A	9.16429	β_1	0.00388
	R_0	-0.05093	β_2	7.07E-05

Table 1:- Parameters of the generated equations for the nonlinear models that calculate the values of d and $1/d^2$ for the 3901 experimental points

Hf 14 .at%	Hf content (Y)	Transformation Temperatures (Kelvin)				$\mid Af - As \mid$ (K)	$\mid Mf - Ms \mid$ (K)	$\mid Af - Ms \mid$ (K)
Processing	Hf_X .at%	Ms	Mf	As	Af	Partial hysteresis	Partial hysteresis	Total hysteresis
Melt Spinning	Hf_{14} - 30 Hz	327.33	317.63	360.74	377.4	16.66	9.7	50.07
	Hf_{14} - 40 Hz	295.62	238.8	299.53	349.08	49.55	56.82	53.46
Plasma arc	Hf_{14} - série 1	363.71	349.74	389.23	414.09	24.86	13.97	50.38
	Hf_{14} - série 2	359.04	302.13	372.69	421.57	48.88	56.91	62.53
Arc melting	Hf_{14} .at%	405.13	363.5	418.47	461.25	42.78	41.63	56.12
Hf 20 .at%	Hf content (Y)	Transformation Temperatures (Kelvin)				$\mid Af - As \mid$ (K)	$\mid Mf - Ms \mid$ (K)	$\mid Af - Ms \mid$ (K)
Processing	Hf_X .at%	Ms	Mf	As	Af	Partial hysteresis	Partial hysteresis	Total hysteresis
Melt Spinning	Hf_{20} - 30 Hz	373.95	360.04	402.34	412.8	10.46	13.91	38.85
	Hf_{20} - 40 Hz	330.34	244.96	293.88	377.09	83.21	85.38	46.75
Plasma arc	Hf_{20} - série 1	396.02	335.23	391.75	449.79	58.04	60.79	53.77
	Hf_{20} - série 2	397.15	316.5	403.78	469.56	65.78	80.65	72.41
Arc melting	Hf_{20} .at%	520.32	444.69	489.61	559.3	69.69	75.63	38.98

Table 2:- Comparison of TTs for compositions Hf_{14} and Hf_{20} .at% (Y = 14 and Y = 20 .at%)

The increase in TT is directly associated with some attributes such as: (*i*) the longer the solidification time, the more conditions there were for grain growth, exceptionally when the grain size in the melt spun tapes was analyzed in the horizontal position. The larger grain size requires more thermal and enthalpy demand for phase transformation in the solid state. In electric arc melting processing, the volume of the liquefied alloy was not converted into a copper mass, but simply accommodated on the surface after the electric arc from the tungsten electrode ceased; (*ii*) in plasma arc fusion, the bulk was poured into a copper mold, reducing the possibility of grain growth, as occurs in melt spinning fusion; (*iii*) in melt spinning solidification, the high speed

with which the liquefied alloy is poured and consequently solidified, associated with the rotating speed of the copper flywheel, prevents grain growth, which was thus analyzed in the vertical position (in the tape thickness) . Hence, the smallest grain size was observed in the tapes whose analyzes were made in the direction of thickness, as shown in Fig 3(b).

Although there is a correlation between TT and grain size, there was no experimental evidence capable of associating the evolution/involution of grain size with the addition of hafnium in the nominal compositions originally adopted.

		Horizontal position				Vertical position			
Hf$_Y$ %.at - Frequency		*Melt Spinning* (or *Melt Spun*)							
	Size (μm)	Mean	Median	Minimum	Maximum	Mean	Median	Min	Max
Hf14 %.at - 30 Hz		50.33	48.96	35.66	67.44	1.75	1.78	1.27	2.35
Hf14 %.at - 40 Hz		25.82	26.56	10.24	36.35	1.17	1.15	0.85	1.52
Hf20 %.at - 30 Hz		32.59	31.76	20.97	46.77	8.66	8.56	5.4	12.93
Hf20 %.at - 40 Hz		22.08	22.15	14.96	34.26	4.5	4.58	1.89	6.23
		Plasma arc fusion (PSPP) – furnace Discovery *All Metal*, brand EDG				Electric arc fusion (*arc melting*)			
Composition	Dimensions (μm)	Mean	Median	Minimum	Maximum	Mean	Median	Min	Max
Hf14 .at%	Length	2.14	2.01	1.38	3.27	32.99	29.28	14.57	58.12
	Width	4.26	4.22	3.06	7.18	20.62	19.11	10.69	47.17
	Perimeter	10.85	10.71	7.8	16.54	94.47	79.43	44.31	197.87
	Area (μm^2)	6.64	6.37	3.97	11.14	503.3	386.49	138.8	1612.61
Hf20 .at%	Length	2.22	2.18	1.62	3.16	14.49	13.29	6.79	27.6
	Width	3.27	3.34	2.38	4.71	9.51	8.59	4.73	18.93
	Perimeter	9.2	9.41	6.51	12.39	65.66	52.74	27.75	184.06
	Area (μm^2)	5.82	6.13	3.05	8.2	91.32	72.44	31.92	278.34

Table 3:- Comparison of the average grain sizes for the compositions Ni$_{50}$Ti$_{36}$Hf$_{14}$ .at% and Ni$_{50}$Ti$_{30}$Hf$_{20}$ .at% in the three adopted processes

As shown in Table 3, the larger grain size was observed in the melt spun tapes analyzed in the horizontal position (in the width direction). This occurred due to the peculiarity of conformation in this processing, which subjects the alloy to a typical slip capable of promoting an expansion of the grain in the horizontal plane, as shown in Fig 3(a).

The high temperature transformation shape memory alloys (HTSMA), which has As > 100 ºC [7], are considered because the most cited fusion processes allow these types of alloys to generate high thermal energy that generally exceeds 3000 ºC. The standardized process for reaching such TT is the electric arc melting, because the torch can reach the limit of 3600 ºC. It is also important to mention that the high level of vacuum achieved by this equipment, which is necessary to avoid any type of oxidation, especially titanium, becomes essential to obtain and ensure typical properties such as, for example, high TT, compositional

homogeneity and increasing/decreasing thermal hysteresis, according to the nominal composition.

In this work it was proven that the same compositions of Ni$_x$Ti$_{x-y}$Hf$_y$ .at% alloys, when also submitted to non-conventional processes of HSTMA alloys (plasma arc and melt spinning), become materials with TT that sometimes are lower than the Ni-Ti alloys themselves. This is because, among the three, electric arc melting is the process that best diffuses the hafnium in the alloy, which ends up promoting a better compositional homogenization, larger grain size, considerable increase in TT and higher incidence of B19' phases (space group P12$_1$/m1).

In the case of plasma arc melting process, there is a thermal limitation of 2500 ºC. As a result, the compositional heterogeneity in these alloys occurs due to the fact that hafnium is not properly spread within the Ni-Ti-Hf alloy, since the melting point of Hf is 2233 ºC. This was

confirmed with the variation of TTs in the two series of samples analyzed.

For the melt spinning process, the alloys were previously arc melted in the form of billets, in order to be able to fuse them in the fast solidification process. This was necessary because it was previously verified that the Melt Spinning equipment would reach a maximum of 1400 ℃ while the thermodynamic equilibrium diagram indicated the demand of approximately 1380 ℃ for the alloy with the highest hafnium content: 20 .at%. Therefore, in this last composition, the thermal limit of the melt spinning equipment was reached.

Analyzing grain size and morphology, it can be said that they are different from each other, considering the three methods of obtaining the ternary alloys studied here. These differences are explained in Table 3. In Melt Spinning

processing, the smallest grain size predominates due to the speed with which the tapes are solidified. The thermodynamic non-equilibrium decreases the time of formation and growth of the grain as much as possible, which is even more accentuated when the rotating speed of the copper flywheel increases (from 18.84 m/s to 25.83 m/s). It is important to note that the mass of 10 g of each sample was poured into a rotary wheel of high cupric mass, which makes this wheel a means of excellent thermal conductivity.

It should also be noted that the grain in the chemically etched tapes occurs in two ways, according to the position that is observed under the microscope: it is larger and rectilinear, in the direction of the width (seen in the horizontal position) and smaller and curvilinear (rounded) , in the direction of thickness (seen in the vertical position), as shown in Fig 3.
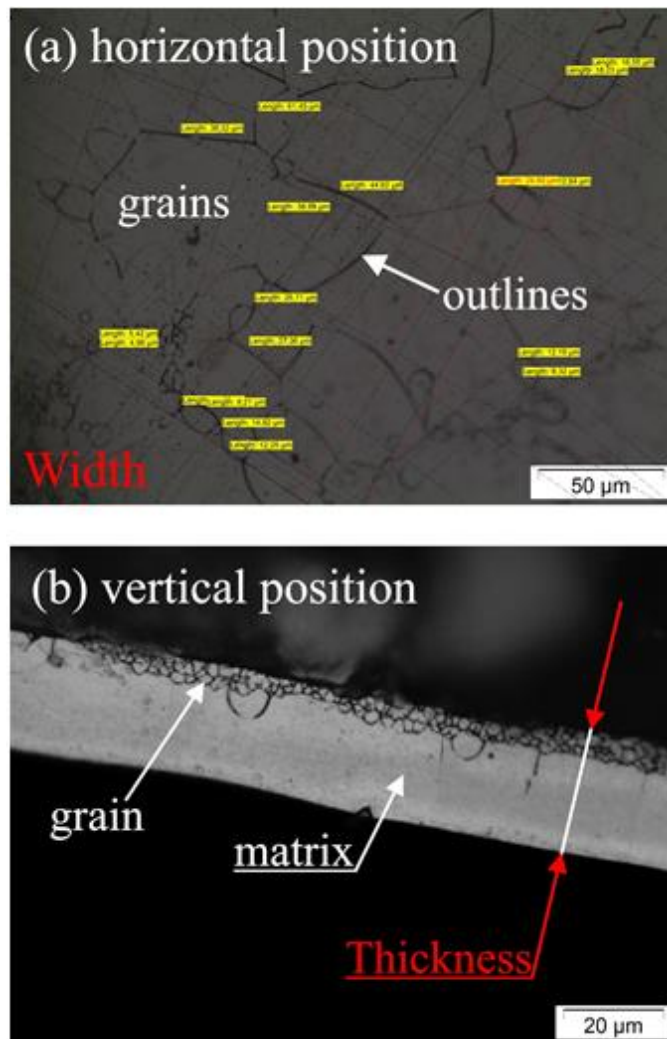

Fig 3:- Optical Microscopy [OM] of the tapes rapidly solidified by melt spinning: (a) horizontal position; (b) vertical position

However, in the vertical position it is possible to differentiate two grains regions: a zone of smaller grains where the liquefied alloy touched the copper flywheel and a zone of slightly larger grains where the liquefied alloy did not touch the flywheel (or copper wheel).

The plasma arc melting process (PSPP method) produces an expansion of the grain in relation to melt spinning, but with superficial, morphological and dimensional irregularities, as shown in Fig 4. This reflects the compositional heterogeneity of the alloys obtained with the Discovery All Metal furnace from EDG. It is also

important to note that a mass of 20 g for each sample was poured into a copper mold whose mass is much smaller than that found in the Melt Spinning process. Comparing the fast solidification and the plasma arc fusion, there was a lower heat flux in the latter process, which favors grain growth. This was confirmed in microscopic observations (OM - optical microscopy and SEM - scanning electron microscopy).
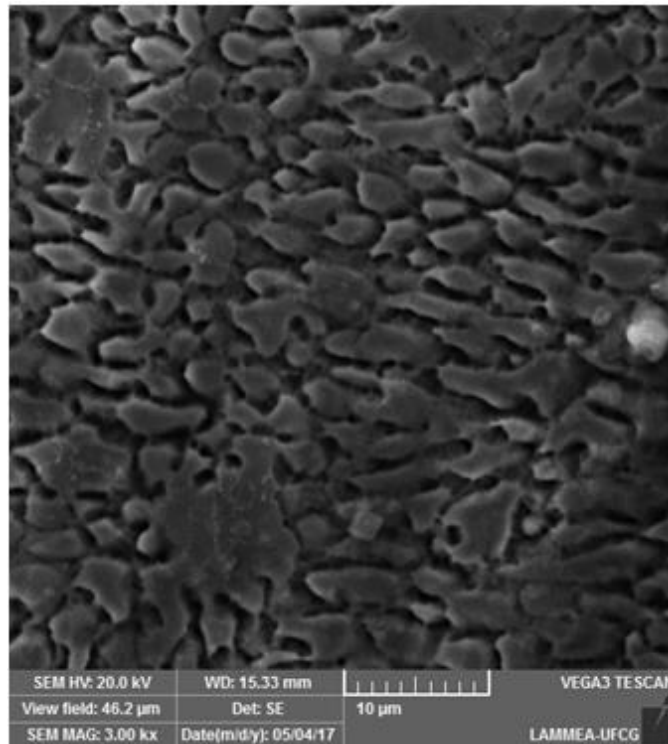

Fig 4:- SEM image of the grains surface of the $Ni_{50}Ti_{36}Hf_{14}$ .at% alloy obtained by plasma arc melting (PSPP method)

However, it is the electric arc melting process that produces larger grains, because of the maximum homogenization that conditions the formation of a denser polycrystalline structure in this alloy. The crystallization time for the electric arc melting is also much longer compared to the other processes because the mass of 10 g for each sample was not poured into a mold/flywheel like in the other two processes, but only solidified after removing the torch.

Therefore, electric arc melting is closest to the thermodynamic equilibrium, which favors grain growth and, therefore, greater repetitive regularity of the B19' martensitic matrix, which has a monoclinic crystalline structure (Pearson symbol mP8). Thereby, melt spinning and plasma processes are not suitable for obtaining Ni-Ti-Hf alloys with EMF considered to be HTSMA

.

III. CONCLUSION

Based on the results presented, considering the three processes adopted in this article, it is possible to draw some conclusions. Regarding thermal properties:

➢ TTs are associated with grain size because the smaller the grain, smaller the amount of thermal energy required to provide a phase change in the solid state. The grain (or matrix) is the area with the highest crystalline mass while the contour is amorphous or predominantly stoichiometric (formed by the combinations Ni-Ti, Ti-Hf, Ni-Hf or Ni-Ti-Hf).

➢ The grain size in the melt spun strips observed in a horizontal position (width direction) is an exception that should not be correlated with the TTs measurements, since the highest average observed, equal to 50.33 µm, does not explains the low TTs on the fast solidification tapes. The expansion of those grains in the horizontal plane was conditioned to the tangential force of the turning of the flywheel in the poured liquefied alloy. Thus, for a TT correlation, only the grains observed in the tapes placed in a vertical position (thickness direction) should be taken into account.

➢ TTs are generally: very low on tapes solidified by melt spinning; low in alloys obtained from plasma arc melting; and high in alloys obtained by electric arc melting. This is related to the grain size, which was found to be smaller in tapes observed in a vertical position (lower average: 1.75 µm) and higher in alloys obtained by electric arc melting (higher average; 32.99 µm).

➢ The increase in TTs is associated with the gradual increase in hafnium (3 .at%) of alloys and tapes, regardless of the processing involved. This increase in TTs is also directly proportional to the volume of crystalline cells in the B19' martensitic phase (monoclinic structures), especially in alloys produced by electric arc melting.

➤ The TTs in NixTix-yHfy .at% alloys of the same nominal compositions is different for each method of production. This is conditioned to the real operational capacities of each furnace used and other operational variables. In addition, thermal levels are a reflection of homogeneity, which is derived from each process and its respective peculiarities.

➤ Partial Thermal Hysteresis (ΔP) are described according to a regular function in rapidly solidified tapes and in alloys obtained by electric arc melting. This property describes a combined homogeneity in the compositions. This does not occur in alloys fused by plasma arc due to their compositional heterogeneity, which was observed in the 2 series of PSPP samples (Plasma Skull Push – Pull).

➤ There was a greater demand for enthalpy energies in alloys produced by electric arc melting (average: 12.00 J/g) due to the better compositional homogenization of the B19' martensitic phase in the five samples analyzed.

According to (micro)structural properties:

➤ The relative degree of crystallinity (Xc) was considered in the three processes: low in the alloys obtained from plasma arc melting (PSPP); medium in the tapes solidified by melt spinning; and higher in electric arc melted alloys.

➤ It was found that $Ni_xTi_{x-y}Hf_y$ .at% alloys and tapes are polycrystalline materials that vary, at room temperature, the amount of cubic, rhombohedral, hexagonal (trigonal axis), monoclinic and orthorhombic structures, whether with binary formations (NiTi) or ternary (NiTiHf).

➤ Non-linear functions were obtained to relate the angle 2θ [º] with the interplanar distance - d (negative exponential function) as well as with the fraction $1/d^2$ (positive quadratic function), which identifies the crystalline structure, regardless of verified phases: R, H, B2, B19 or B19'. In all cases there was an excellent statistical adjustment ($R^2 > 0.98$).

➤ The descriptive statistics produced from the micrometric sizes of the grains served to visualize, with 30 samples of data for each variable, a greater precision in the conclusions about this attribute that is generally treated superficially.

➤ Considering each process individually, there was a high incidence of indexation (H K L), since in each process they were indexed, adding the peaks of all samples: 2233 peaks in the PSPP process (5 samples), 2780 peaks in the melt spin process (8 samples) and 613 B19'peaks in the electric arc process (5 samples). Altogether 5626 peaks were indexed. This was possible because the average relative degree of crystallinity (Xc) has always exceeded 50%, for the respective processes: 55.73%, 60.64% and 63.63%.

REFERENCES

[1]. Buytoz, S., et al., *Microstructure Analysis and Thermal Characteristics of NiTiHf Shape Memory Alloy with Different Composition.* Metals and Materials International, 2019.

[2]. Araújo, C.J.d., et al., *Fabrication of shape memory alloys using the plasma skull push–pull process.* Journal of Materials Processing Technology, 2009. **209**(7): p. 3657 - 3664.

[3]. Rivlin, Z., et al., *Evaluation of the contact angle in rapid solidification by melt spinning.* Materials Science and Engineering: A, 1996. **211**(1): p. 82 - 86.

[4]. Koichiro, K., *Ash melting system and reuse of products by arc processing.* Waste Management, 1996. **16**(5): p. 423 - 430.

[5]. Zarinejad, M., Y. Liu, and T.J. White, *The crystal chemistry of martensite in NiTiHf shape memory alloys.* Intermetallics, 2008. **16**(7): p. 876-883.

[6]. Kacher, J., et al., *Bragg's Law diffraction simulations for electron backscatter diffraction analysis.* Ultramicroscopy, 2009. **109**(9): p. 1148-1156.

[7]. Ma, J., I. Karaman, and R.D. Noebe, *High temperature shape memory alloys.* International Materials Reviews, 2010. **55**(5): p. 257-315.